

A Joint Beamforming Design and Integrated CPM-LFM Signal for Dual-functional Radar-communication Systems

Yu Cao, *Student Member, IEEE*, Qi-Yue Yu, *Senior Member, IEEE*

Abstract—The dual-functional radar-communication (DFRC) system is an attractive technique, since it can support both wireless communications and radar by a unified hardware platform with real-time cooperation. Considering the appealing feature of multiple beams, this paper proposes a precoding scheme that simultaneously support multiuser transmission and target detection, with an integrated continuous phase modulation (CPM) and linear frequency modulation (LFM) signal, based on the designed dual mode framework. Similarly to the conception of communication rate, this paper defines radar rate to unify the DFRC system. Then, the maximum sum-rate that includes both the communication and radar rates is set to be the objective function. Regarding as the optimal issue is non-convex, the optimal problem is divided into two sub-issues, one is the user selection issue, and the other is the joint beamforming design and power allocation issue. A successive maximum iteration (SMI) algorithm is presented for the former issue, which can balance the performances between the sum-rate and complexity; and maximum minimization Lagrange multiplier (MMLM) iteration algorithm is utilized to solve the latter optimal issue. Moreover, we deduce the spectrum characteristic, bit error rate (BER) and ambiguity function (AF) for the proposed system. Simulation results show that our proposed system can provide appreciated sum-rate than the classical schemes, validating the efficiency of the proposed system.

Index Terms—Dual-functional radar-communication (DFRC), precoding, continuous phase modulation (CPM), linear frequency modulation (LFM), maximum minimization Lagrange multiplier (MMLM), user selection.

I. INTRODUCTION

CURRENTLY, the joint communication and radar (JCR) system has been widely researched in both academic and industry [1], since it can simultaneously satisfy the data transmission and target detection, providing real-time information sharing. Therefore, the JCR system has been applied into indoor positioning [2], UAV networks [3], vehicle networks [4], and etc. Especially, the JCR system is an appealing choice for seamless connectivity to serve multiple communication users and achieve the target information. Compared to the classical single radar or communication equipment, it has advantages in terms of cost, size, power consumption, spectrum usage, and etc [5] [6].

The work presented in this paper was supported by the National Natural Science Foundation of China under Grand No. 62071148, and partly supported by the Natural Science Foundation of Heilongjiang Province of China under Grand No. YQ2019F009.(Corresponding author: Qiyue Yu).

Y. Cao and Q.-Y. Yu are with the Communication Research Center, Harbin Institute of Technology, China. (email: {yucuo, yuqiyue}@hit.edu.cn).

The concept of JCR was first proposed by Space Shuttle program of National Aeronautics and Space Administration (NASA) in the late 1970's [7]. The initial goal was to integrate the electronic warfare (EW) of communication and radar functions into the antenna array (AA) for resource sharing, mainly used in military scenarios. Slowly, JCR is applied into civil area, e.g., advanced driver assistance systems (ADAS) [8]. In airborne areas, [9] merges the communication system and the synthetic aperture radar (SAR) by the space time coding (STC) scheme.

The prospective research directions of JCR mainly include radar-communication coexistence system (RCC) and dual-functional radar-communication (DFRC) [10]. The RCC system emphasizes on the coexistence of communication and radar system that mainly develops efficient interference management techniques, including null space signal projection, transmit waveform design, power-efficient pattern design and dynamic spectrum allocation [11]-[14]. [11] proposes a null space projection method to eliminate the interferences of the RCC system, with the knowledge of the channel state information (CSI). [12] designs transmit waveforms by space-time code based on the controllable degrees of freedom to reduce the self-interferences of the RCC receiver. For the signal side-lobe interference control aspect, [13] presents a Riemann gradient conjugate power budget waveform design method to reduce the influence of side-lobe interference of a multiple input multiple output (MIMO) RCC system. In [14], the authors aim to minimize the downlink multiuser interference by using branch-and-bound dynamic spectrum allocation method.

On the other hand, the DFRC focuses on the cooperation of communication and radar systems, and generally adopts integrated signal to improve the performances of both communication and radar [15]. There are many prospective research directions of DFRC, especially, beamforming design and integrated signal construction are two of the appealing ones [16].

There are many works on beamforming design of the DFRC system [17]-[21]. In [17], the authors present an optimal beamforming method to minimize the downlink multiuser interference, and further propose a weighted beam-pattern for a flexible trade-off between the performance of radar and communication. In [18], the authors design a beamformer that matches the radar's beam-pattern; moreover, it satisfies the communication performance relied on the null-space criterion with the constraint of signal-to-interference-plus-noise ratio

(SINR). [19] presents a predictive beamforming scheme to enhance angle estimation accuracy by the maximum posteriori probability criterion, which can acquire the location and track the information of a vehicular system. In [20], the authors present a hybrid beamformer based on the minimum mean square error (MMSE) criterion, which can enhance the achievable sum-rate significantly. [21] presents the transmit beamforming scheme based on the maximum SINR criterion, which optimizes both the radar transmit beam pattern and communication rate.

Besides the beamforming topic, signal waveforms designing is another hot topic. To combine the communication and radar waveforms, there are generally three major categories, they are orthogonal frequency division multiplexing (OFDM), frequency modulation (FM) and spread spectrum (SS) [22]. In [23], the author proposes an OFDM queue scheduling model, taking both the network stability and radar detection performance into consideration. [24] proposes a novel code-division OFDM system to provide high spectrum efficiency and robust radar sensing performances. The linear frequency modulation (LFM) is widely considered in DFRC systems, since it provides a larger detection range and a higher range resolution for radar detection [25]. Phase-coded frequency modulation can mitigate the impact of Doppler shift, thus it is suitable for high speed target detection [26]. In [27], the authors combine the low density parity check (LDPC) codes with LFM signals for a DFRC system, which can provide a better BER than the LFM signal. The combination of continue phase modulation (CPM) and LFM can reduce the influence of side lobes [28], thus improve the power and spectrum efficiency. As for spread spectrum signal, the direct sequence (DS) can provide well-behaved auto- and cross-correlation properties to separate the radar and communication information perfectly [29].

Obviously, a joint design of beamforming and signal-form for a DFRC system is a prospective research topic, since it can take signal processing gains to avoid interferences and improve the spectrum efficiency. [30] considers the Hadamard-Walsh orthogonal codes with minimum variance distortionless response (MVDR) beamforming algorithm to achieve a better jamming and interference mitigation capability. [31] presents a zero-forcing beamforming algorithm to transmit the independent radar waveforms and communication symbols simultaneously.

Considering the attractive feature of the joint design, this paper presents a joint beamforming and integrated CPM-LFM signal for a DFRC system. The major advantages of CPM are two aspects: one is the continuity of signal phase that improves the spectrum; and the other is that the Viterbi decoding (or demodulation) provides better BER performance. Furthermore, LFM signal is widely used in radar detection, since it has large time-bandwidth product, which can effectively solve the contradiction between resolution and measuring accuracy. Thus, the integrated CPM-LFM signal is an appealing attempt for a JCR system. To further improve the performance of CPM-LFM, antenna array is jointly considered in this paper, and the precoder is designed based on the maximum sum-rate that includes both communication and radar rates as our

objective function. The contributions of this paper are mainly summarized as three aspects:

- 1) We present a joint beamforming design and integrated CPM-LFM signal for JCR systems. The designed dual mode framework that is consisted of static and dynamic beams can simultaneously support multiuser transmission and target detection;
- 2) Based on the definition of radar rate, we set maximum sum-rate as our objective function that can be proved to be a non-convex optimal issue. To find the optimal solution, the entire problem is divided into two sub-issues, which are user selection and beamforming weights design with power allocation. A successive maximum iteration algorithm is proposed for the user selection, and the maximum minimization Lagrange multiplier (MMLM) is proposed to solve the latter one; and
- 3) Theoretical analysis are presented for the proposed system, including spectrum, bit error rate (BER) and ambiguity function (AF) analysis. Numerical results verify the validity of the proposed system.

The remainder of this paper is organized as follows. Section II presents the system model and the dual mode framework of the proposed system. In Section III, the transmitter and receiver of the proposed system is described in details. An objective function and its solutions are deduced in Section IV. Section V discusses the spectrum characteristic, BER and AF. Simulation results are given in Section VI, following with some conclusion remarks in Section VII.

II. PRELIMINARY

In this paper, denote \mathbb{B} and \mathbb{C} by binary field and complex field. Let x , \mathbf{x} and \mathbf{X} be a scalar, a vector and a matrix, respectively. The transposition, conjugate and conjugate transpose of \mathbf{x} are denoted by \mathbf{x}^T , \mathbf{x}^* and \mathbf{x}^H respectively. Define $*$ as convolution operation, and $\|\mathbf{x}\|_2$ represents vector Euclidean norm. $\mathcal{CN}(\mu, \sigma^2)$ indicates the complex Gaussian distribution with mean μ and covariance σ^2 . $\text{Re}(x)$ means the real part of the complex number x . $\mathbb{E}(\mathbf{x})$ means the expectation of a random sequence \mathbf{x} . \mathbf{I}_n is n -dimensional identity matrix, $\text{Det}(\mathbf{X})$ represents the determinant of \mathbf{X} , $\text{tr}(\mathbf{X})$ means the a trace of \mathbf{X} , $\text{Diag}(\mathbf{X})$ means a diagonal matrix that is composed of the diagonal element of \mathbf{X} , and $\text{vec}(\mathbf{X})$ indicates converting a matrix \mathbf{X} to a vector by vectorizing columns from the left side to the right side of \mathbf{X} .

A. System model

Assume the base station (BS) is equipped with N_t transmit antennas and N_r received antennas, which form transmit and received antenna arrays for both communication and radar functions. There are totally U user equipments (UEs), where $U \gg N_t$, and each UE holds a single antenna. Since the BS cannot serve all the UEs simultaneously, we assume that K UEs are selected from U , where $K \leq N_t$. The locations of all the U UEs are assumed to be available at the BS. Let the range, speed, elevation and azimuth angle of the target (TA) be d_T , v_T and (θ_T, φ_T) respectively, which will be estimated

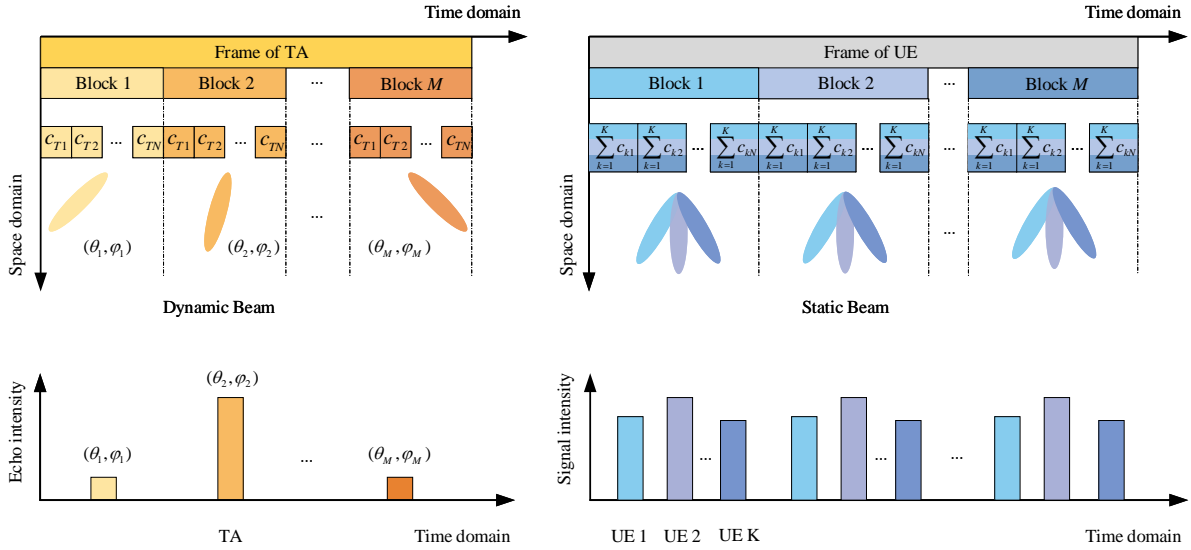


Fig. 1: A dual mode framework of a DFRC system, including time-sharing scanning mode given in (a) and fixed-direction mode given in (b).

by the radar at the BS. The ranges of elevation θ_T and azimuth φ_T are respectively $(0, \pi/2)$ and $(0, 2\pi)$.

The transmit antennas of the BS is set to be a uniform rectangular array (URA) [32], whose element owns a separate phase shifter, providing a three-dimensional (3D) beamforming from elevation and azimuth dimensions. Suppose the numbers of the elements of the transmit URA placed along the X-axis and Y-axis are respectively N_{tx} and N_{ty} , indicating $N_t = N_{tx} \times N_{ty}$. Let the distances between adjacent antenna elements of X-axis and Y-axis be d_x and d_y respectively. Denote the label of each transmit antenna element by (n_{tx}, n_{ty}) , where $1 \leq n_{tx} \leq N_{tx}$ and $1 \leq n_{ty} \leq N_{ty}$. The label of the n_t th element can be expressed as $n_t = (n_{ty} - 1)N_{tx} + n_{tx}$, where $1 \leq n_t \leq N_t$.

Similarly, the received antenna array of the BS is also set to be a URA, and the elements of the received URA are respectively N_{rx} and N_{ry} , i.e., $N_r = N_{rx} \times N_{ry}$. The label of the n_r th received antenna is $n_r = (n_{ry} - 1)N_{rx} + n_{rx}$, where $1 \leq n_{rx} \leq N_{rx}$, $1 \leq n_{ry} \leq N_{ry}$ and $1 \leq n_r \leq N_r$.

B. Framework

The transmit URA of the BS should simultaneously provide different beams for both UEs' communication and TA's detection. The UEs' angle information are available at the BS, and the beamforming algorithms are determined by these angle information. On contrast, the TA's angle information is unknown, which needs to be estimated. Thus, the transmit URA of the BS is consist of two types of beams, one is dynamic beams for TA's searching, and the other is static beams for UEs' communications, as shown in Fig. 1.

Through dynamic beam scanning, both the position and speed information of the TA are expected to be estimated. Meanwhile, UEs are served by the static beams. Because of the different roles of dynamic and static beams, this paper proposes a dual mode framework that is consisted of dynamic time-sharing scanning mode and static fixed-direction mode.

Assume one frame is consisted of M blocks and each block includes N symbols. It is noted that M is equal to the product of M_e and M_a , i.e., $M_e = \frac{\pi}{2\delta_\theta}$ and $M_a = \frac{2\pi}{\delta_\varphi}$, where δ_θ and δ_φ are beamwidth in elevation and azimuth dimensions. Therefore, the TA detection precision relays on the value of M . A large M indicates a higher precision, at the cost of longer scanning time. The dynamic beam alters its direction every block time, thus named as "dynamic". During one frame time, there are totally M dynamic beams. Conversely, the static beams keep the directions during the entire frame time, as if "static". Dynamic beam utilize time-sharing scanning mode to detect the position and speed of a moving TA. The scanning direction (θ_m, φ_m) of the m th block, where $1 \leq m \leq M$, keeps as a constant during the m th block. If the reflected echo signal of the m th dynamic beam that is larger than the threshold, the TA is estimated to be at the direction (θ_m, φ_m) . If the reflected echo signal of the m th dynamic beam is smaller than the threshold, there is no TA exists.

III. DESIGN OF JOINT BEAMFORMING AND CPM-LFM INTEGRATED WAVEFORM

This section presents a joint beamforming and CPM-LFM integrated system that is designed based on the dual mode framework, as shown in Fig. 2.

A. Transmit signals of the BS

To detect whether there is a TA or not, a pilot sequence is transmitted by the m th dynamic beam, and defined by $\mathbf{a}_T = [a_{T,1}, a_{T,2}, \dots, a_{T,N \log \mathcal{M}}] \in \mathbb{B}^{1 \times N \log \mathcal{M}}$, where \mathcal{M} is modulation order of a M -ary amplitude shift keying (MASK), and the subscript "T" indicates the sequence (or signal) for the TA detection. Suppose K selected UEs are simultaneously served by the static beams, where $1 \leq K \leq U$, define the transmit binary data sequence of the k th UE by $\mathbf{a}_k = [a_{k,1}, a_{k,2}, \dots, a_{k,N \log \mathcal{M}}] \in \mathbb{B}^{1 \times N \log \mathcal{M}}$, where $1 \leq$

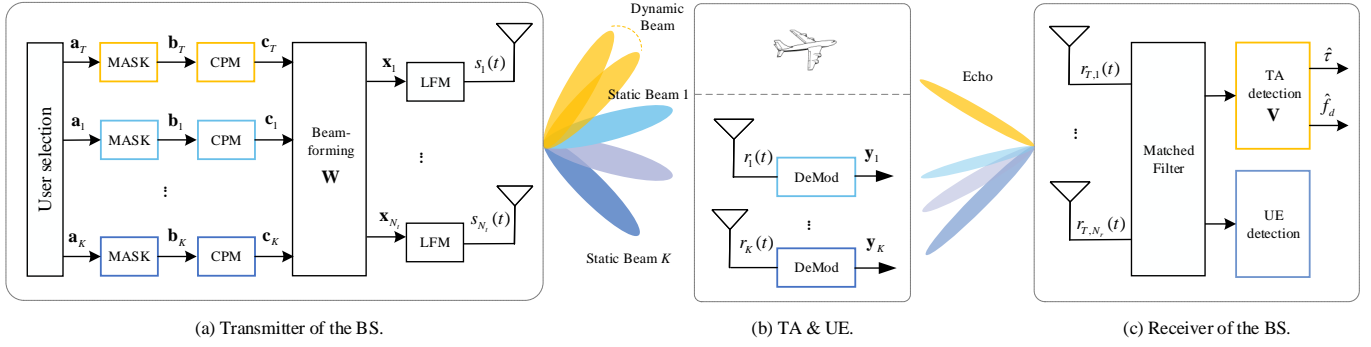


Fig. 2: A diagram of the transmitter and receiver of our proposed DFRC system, where “DeMod” indicates demodulation. There are N_t transmit antennas, and N_r received antennas at the BS. Each UE is equipped with one antenna.

$k \leq K$. The binary data sequences are firstly passed to the MASK mapper, and achieved complex signals $\mathbf{b}_T = [b_{T,1}, b_{T,2}, \dots, b_{T,N}] \in \mathbb{C}^{1 \times N}$ and $\mathbf{b}_k = [b_{k,1}, b_{k,2}, \dots, b_{k,N}] \in \mathbb{C}^{1 \times N}$.

Then \mathbf{b}_T and \mathbf{b}_k are passed to the CPM modulator. In order to ensure the phase continuity, the phase of the baseband signal of TA and the k th UE at the n th symbol duration T_s are calculated as

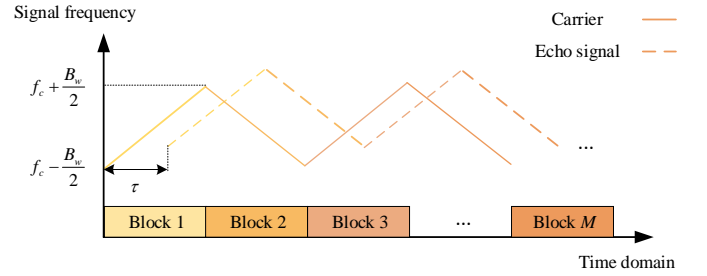
$$\begin{aligned} \beta_{T,n} &= \sum_{i=1}^n b_{T,i} h \pi, \\ \beta_{k,n} &= \sum_{i=1}^n b_{k,i} h \pi, \end{aligned} \quad (1)$$

where $1 \leq n \leq N$ and the parameter h is modulation index [33]. The corresponding phase vectors of the TA and the k th UE are $\boldsymbol{\beta}_T = [\beta_{T,1}, \beta_{T,2}, \dots, \beta_{T,N}]$ and $\boldsymbol{\beta}_k = [\beta_{k,1}, \beta_{k,2}, \dots, \beta_{k,N}]$, respectively. Thus, the baseband signals of CPM are obtained as $\mathbf{c}_T = e^{j\boldsymbol{\beta}_T} \in \mathbb{C}^{1 \times N}$ and $\mathbf{c}_k = e^{j\boldsymbol{\beta}_k} \in \mathbb{C}^{1 \times N}$, forming the transmit data matrix $\mathbf{C} = [\mathbf{c}_T^T, \mathbf{c}_1^T, \dots, \mathbf{c}_K^T]^T \in \mathbb{C}^{(K+1) \times N}$.

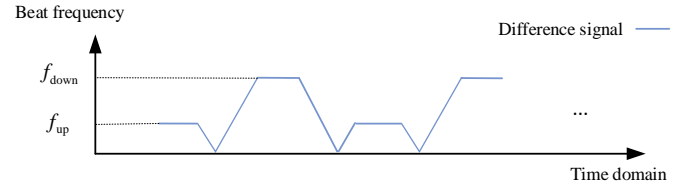
In this paper, the transmit URA adopts fully connection structure. Suppose that the beamforming weight vectors of the TA and the k th UE are defined by $\mathbf{w}_T = [w_{1,T}, \dots, w_{n_t,T}, \dots, w_{N_t,T}] \in \mathbb{C}^{N_t \times 1}$ and $\mathbf{w}_k = [w_{1,k}, \dots, w_{n_t,k}, \dots, w_{N_t,k}] \in \mathbb{C}^{N_t \times 1}$, thus the precoding matrix can be represented as $\mathbf{W} = [\mathbf{w}_T, \mathbf{w}_1, \dots, \mathbf{w}_K] \in \mathbb{C}^{N_t \times (K+1)}$. Assume the transmit power of the TA and k th UE are P_T and P_k respectively, and the corresponding power allocation matrix is $\mathbf{P} = \text{Diag}(P_T, P_1, \dots, P_K) \in \mathbb{C}^{(K+1) \times (K+1)}$. After precoding and power allocation, the transmit data on the n_t th antenna is represented as

$$\mathbf{x}_{n_t} = \sqrt{P_T} w_{n_t,T} \mathbf{c}_T + \sum_{k=1}^K \sqrt{P_k} w_{n_t,k} \mathbf{c}_k, \quad (2)$$

where $\mathbf{x}_{n_t} = [x_{n_t,1}, \dots, x_{n_t,n}, \dots, x_{n_t,N}] \in \mathbb{C}^{1 \times N}$ and $1 \leq n_t \leq N_t$. The baseband signal \mathbf{x}_{n_t} is passed to the filter, and modulated to the carrier frequency f_c to form LFM waveforms, then the corresponding integrated bandpass sig-



(a) The relationship between signal frequency and symbol duration.



(b) The relationship between beat frequency and symbol duration.

Fig. 3: The frequency variations of the carrier, echo signal and difference signal during M blocks, where τ is the latency, f_c is the center frequency and B_w is the sweep bandwidth.

nal is $\mathbf{s}(t) = [s_1(t), \dots, s_{n_t}(t), \dots, s_{N_t}(t)]^T$, where $s_{n_t}(t)$ is transmitted on the n_t th antenna, which is given by

$$s_{n_t}(t) = \sum_{n=1}^N x_{n_t,n} g(t - (n-1)T_s) e^{j(2\pi f_c t + \pi \mu t^2)}, \quad (3)$$

where $(n-1)T_s \leq t \leq nT_s$. $g(t)$ is the transmit pulse, which can be rectangular pulse, raised cosine pulse, Gaussian pulse, and etc [34]. μ is the chirp rate of the bandpass integrated signal [35]. If $\mu > 0$, it is a up-chirp signal; otherwise it is a down-chirp signal.

Due to the feature of the triangular wave, the chirp rate is a constant value during one block time T_B , i.e., $T_B = NT_s$, and the chirp rate changes to its opposite value during the next block time. As shown in Fig. 3 (a), there are M blocks, and the chirp rates of the odd and even blocks are respectively μ and $-\mu$, which are also called up-chirp and down-chirp blocks.

According to the chirp rate μ and block time T_B , the sweep bandwidth B_w is given by

$$B_w = \mu T_B = \mu N T_s, \quad (4)$$

$$\begin{aligned}\mathbf{a}_{tx}(\theta_k, \varphi_k) &= \frac{1}{\sqrt{N_{tx}}} \left[1, e^{j2\pi \frac{d_x}{\lambda} \cos \theta_k \cos \varphi_k}, \dots, e^{j2\pi(N_{tx}-1) \frac{d_x}{\lambda} \cos \theta_k \cos \varphi_k} \right], \\ \mathbf{a}_{ty}(\theta_k, \varphi_k) &= \frac{1}{\sqrt{N_{ty}}} \left[1, e^{j2\pi \frac{d_y}{\lambda} \cos \theta_k \sin \varphi_k}, \dots, e^{j2\pi(N_{ty}-1) \frac{d_y}{\lambda} \cos \theta_k \sin \varphi_k} \right].\end{aligned}\quad (6)$$

which indicates the highest frequency and lowest frequency of the transmit signals are respectively $f_c + B_w/2$ and $f_c - B_w/2$.

B. Received signals at each UE

The integrated signal is then transmitted to the fading channel. Assume that the elevation and azimuth of the k th UE θ_k and φ_k are perfectly known at the BS, and the ranges of elevation θ_k and azimuth φ_k are respectively $(\pi/2, \pi)$ and $(0, 2\pi)$. Thus, the CSI $\mathbf{h}_k \in \mathbb{C}^{1 \times N_t}$ between the k th UE and BS is modeled as

$$\mathbf{h}_k = \sqrt{(d_k/d_0)^{-\alpha}} \delta_k \mathbf{a}_t(\theta_k, \varphi_k), \quad (5)$$

where d_k is the distance from the BS to the k th UE, d_0 is the reference distance, $d_k \geq d_0$, α is the path loss exponent, δ_k indicates shadowing effect that is a zero mean and σ_δ variance log-normal random variable. $\mathbf{a}_t(\theta_k, \varphi_k) = \text{vec}(\mathbf{a}_{tx}(\theta_k, \varphi_k) \mathbf{a}_{ty}^T(\theta_k, \varphi_k)) \in \mathbb{C}^{1 \times N_t}$ is the transmit steering vector from the BS to the k th UE [36], which are given by (6), where $\lambda = \frac{c}{f_c}$ stands for the wavelength.

At the receiver of the k th UE, the received bandpass signal $r_k(t)$ can be given as

$$r_k(t) = \mathbf{h}_k \mathbf{s}(t) + n_k(t). \quad (7)$$

The received bandpass signal $r_k(t)$ is coherent demodulated and passed through the lowpass filter, the equivalent baseband signal $\mathbf{y}_k \in \mathbb{C}^{1 \times N}$ is

$$\begin{aligned}\mathbf{y}_k &= \sqrt{P_k} \mathbf{h}_k \mathbf{w}_k \mathbf{c}_k + \sqrt{P_T} \mathbf{h}_k \mathbf{w}_T \mathbf{c}_T \\ &+ \sum_{i=1, i \neq k}^K \sqrt{P_i} \mathbf{h}_k \mathbf{w}_i \mathbf{c}_i + \mathbf{n}_k,\end{aligned}\quad (8)$$

where \mathbf{n}_k is the complex additive white Gaussian noise (AWGN) obeying $\mathcal{CN}(0, \sigma_k^2)$ with variance σ_k^2 . The first item is our expected signal, the second and the third items are both interferences, which can be eliminated by designing precoding matrix \mathbf{X} , and the last one is noise.

C. Received signals at the BS

If there is a TA at the location of (θ_m, φ_m) during the m th block time, an echo signal is feedback to the BS. The received URA of the BS is used to acquire the echo signals of the TA. The steering vectors from the BS to the TA is denoted by $\mathbf{a}_t(\theta_m, \varphi_m) = \text{vec}(\mathbf{a}_{tx}^T(\theta_m, \varphi_m) \mathbf{a}_{ty}(\theta_m, \varphi_m)) \in \mathbb{C}^{1 \times N_t}$, and from the TA to BS is $\mathbf{a}_r(\theta_m, \varphi_m) = \text{vec}(\mathbf{a}_{rx}^T(\theta_m, \varphi_m) \mathbf{a}_{ry}(\theta_m, \varphi_m)) \in \mathbb{C}^{1 \times N_r}$. Let $\mathbf{A} = [\mathbf{a}_r^T(\theta_m, \varphi_m) \mathbf{a}_t(\theta_m, \varphi_m)] \in \mathbb{C}^{N_r \times N_t}$, and $\mathbf{A}_K = [\mathbf{a}_r^T(\theta_1, \varphi_1), \mathbf{a}_r^T(\theta_2, \varphi_2), \dots, \mathbf{a}_r^T(\theta_K, \varphi_K)] \in \mathbb{C}^{N_r \times K}$, where $\mathbf{a}_r^T(\theta_k, \varphi_k)$ is the steering vector from the k th UE to the BS.

Thus the received bandpass signal at the BS is

$$\mathbf{r}(t) = \mathcal{L} \mathbf{A} \mathbf{s}(t - \tau) e^{j2\pi f_d t} + \mathbf{A}_K \mathbf{I}_K(t) + \mathbf{n}_T(t), \quad (9)$$

where $\mathbf{r}(t) = [r_1(t), \dots, r_{n_r}(t), \dots, r_{N_r}(t)]^T$, $\mathcal{L} = \sqrt{\mathcal{L}_T \eta_T}$ is the gain of echo signal, \mathcal{L}_T is the propagation attenuation and η_T represents radar cross section (RCS). τ and f_d are respectively latency and Doppler frequency of the TA, which are need to be estimated. Let $\mathbf{I}_K = [I_1(t), I_2(t), \dots, I_K(t)]$, where $I_k(t)$ is the signal of the k th UE, which is viewed as interferences for the TA detection, the power of which satisfy $\mathbb{E}(|I_k(t)|^2) = 1$. $\mathbf{n}_T(t)$ is the complex AWGN obey $\mathcal{CN}(0, \sigma^2)$ with variance σ^2 .

Define the processing vector of the BS by $\mathbf{V} \in \mathbb{C}^{1 \times N_r}$, thus, we have

$$\begin{aligned}\mathbf{y}(t) &= \mathbf{V} \mathbf{r}(t), \\ &= \mathcal{L} \mathbf{V} \mathbf{A} \mathbf{W} \mathbf{C} \cdot e^{j[2\pi f_c(t-\tau) + \pi \mu(t-\tau)^2 + 2\pi f_d t]} \\ &+ \mathbf{V} \mathbf{A}_K \mathbf{I}_K(t) + \mathbf{n}(t),\end{aligned}\quad (10)$$

where $\mathbf{n}(t) = \mathbf{V} \mathbf{n}_T(t)$ is the equivalent noise after signal processing.

Define the received difference signal $\mathbf{d}_r(t)$ by the low-pass signal of the product of the echo signal $\mathbf{y}(t)$ and the coherence frequency carrier, i.e., $\mathbf{d}_r(t) = \text{LPF}[\mathbf{y}(t) \cdot e^{j(2\pi f_c t + \pi \mu t^2)}]$, where LPF represents low-pass filter. The frequencies of $\mathbf{d}_r(t)$ are defined by beat frequencies, including f_{up} and f_{down} , which are respectively calculated in the up-chirp and down-chirp stages, as shown in Fig. 3 (b). In each up-chirp block, the frequency of the echo signal is lower than the carrier owing to the influence of latency and Doppler frequency, while in the down-chirp block, the frequency of the echo signal is higher than the carrier.

Thereby, during the up-chirp stage, the received difference signal $\mathbf{d}_{r,\text{up}}(t)$ can be expressed as

$$\begin{aligned}\mathbf{d}_{r,\text{up}}(t) &= \text{LPF} \left[\text{Re}(\mathbf{y}(t)) \cdot \text{Re}(e^{j(2\pi f_c t + \pi \mu t^2)}) \right], \\ &= \mathcal{L} \mathbf{V} \mathbf{A} \mathbf{W} \mathbf{C} \cdot e^{j[2\pi(\mu\tau - f_d)t + 2\pi(f_c\tau + \frac{1}{2}\mu\tau)\tau]} \\ &+ \mathbf{V} \mathbf{A}_K \mathbf{I}_K(t) + \mathbf{n}(t),\end{aligned}\quad (11)$$

where the beat frequency of the up-chirp stage is $f_{\text{up}} = \mu\tau - f_d$. Similarly, it is able to derive the received difference signal of the down-chirp stage as

$$\begin{aligned}\mathbf{d}_{r,\text{down}}(t) &= \text{LPF} \left[\text{Re}(\mathbf{y}(t)) \cdot \text{Re}(e^{j(2\pi f_c t - \pi \mu t^2)}) \right], \\ &= \mathcal{L} \mathbf{V} \mathbf{A} \mathbf{W} \mathbf{C} \cdot e^{j[2\pi(\mu\tau + f_d)t - 2\pi(f_c\tau + \frac{1}{2}\mu\tau)\tau]} \\ &+ \mathbf{V} \mathbf{A}_K \mathbf{I}_K(t) + \mathbf{n}(t),\end{aligned}\quad (12)$$

with the beat frequency of the down-chirp stage as $f_{\text{down}} = \mu\tau + f_d$.

The latency and distance between the BS and TA can be calculated as $\tau = \frac{f_{\text{up}} + f_{\text{down}}}{\mu}$ and $d_T = \frac{c\tau}{2}$, respectively. The Doppler frequency is equal to $f_d = \frac{f_{\text{down}} - f_{\text{up}}}{2}$, and the corresponding radial velocity of the TA is $v_T = \frac{\lambda f_d}{2}$.

Obviously, the latency and Doppler frequency can be exactly estimated without estimation error, if the sweep bandwidth and transmit pulse bandwidth satisfy the resolutions of the requirements. However, the matrix \mathbf{W} and vector \mathbf{V} affect the received power of TA, how to design \mathbf{W} and \mathbf{V} is presented in the following section.

IV. A JOINT BEAMFORMING AND RESOURCE ALLOCATION ALGORITHM

To design the precoding matrix \mathbf{W} and processing vector \mathbf{V} , this section sets the maximum sum-rate as our objective function. Actually, the sum-rate consists of both communication rate and radar rate. It is important to denote a unified sum-rate of a DFRC system. As known, communication sum-rate (or channel capacity) is widely used in communication systems, which indicates the quality of a communication system. To unify the communication and radar systems, we present a concept of radar rate, similarly to the conception of communication rate. Thus, this paper exploits the maximum sum-rate that includes both communication and radar rates as our objective function.

A. Communication rate and radar rate

This paper only considers the downlink multiuser channel capacities between the BS and the UEs as the communication rate. Recalling (8), the SINR of the k th UE can be expressed as

$$\gamma_k = \frac{P_k |\mathbf{h}_k \mathbf{w}_k|^2}{\left| \sqrt{P_T} \mathbf{h}_k \mathbf{w}_T + \sum_{i=1, i \neq k}^K \sqrt{P_i} \mathbf{h}_k \mathbf{w}_i \right|^2 + \sigma_k^2}, \quad (13)$$

where $P_k |\mathbf{h}_k \mathbf{w}_k|^2$ and $\left| \sqrt{P_T} \mathbf{h}_k \mathbf{w}_T + \sum_{i=1, i \neq k}^K \sqrt{P_i} \mathbf{h}_k \mathbf{w}_i \right|^2$ are respectively the power of received signal and interference of the k th UE. Thus, the communication rate of all the UEs is equal to

$$R_{\text{com}} = \sum_{k=1}^K \log_2(1 + \gamma_k), \quad (14)$$

where the subscript ‘‘com’’ of R_{com} stands for communication system.

Whether a TA exists or not, it is determined by the received power of TA at the BS. According to the definition of radar equation [37], if the received power of TA is greater than the minimum detection power, i.e. P_{th} , the TA can be detected. According to (11), the SINR of the TA is calculated as

$$\gamma_T = \frac{\mathcal{E}_{\text{rad}} \mathbf{V} \mathbf{Z} \mathbf{W} \mathbf{W}^H \mathbf{Z}^H \mathbf{V}^H}{\mathbf{V} \mathbf{A}_K \mathbf{A}_K^H \mathbf{V}^H + \mathbf{V} \mathbf{V}^H \sigma^2}, \quad (15)$$

where $\mathbf{Z} = \mathcal{L} \mathbf{A} e^{j(2\pi f_c \tau + \pi \mu \tau^2)}$, $\mathcal{E}_{\text{rad}} = \mathbb{E}[\mathbf{C} \mathbf{C}^H]$ is the power of radar transmit pilot sequence, and the term $\mathbf{V} \mathbf{A}_K \mathbf{A}_K^H \mathbf{V}^H$ indicates the interferences of other UEs.

Similarly to the concept of communication rate, we define the radar rate by

$$R_{\text{rad}} = \log_2(1 + \gamma_T), \quad (16)$$

where the subscript ‘‘rad’’ stands for radar, and the radar rate is affected by \mathbf{V} and \mathbf{W} . Obviously, the defined radar rate can reflect the target detection performance, a large R_{rad} stands for a better detection performance.

B. Objective function

In order to ensure both the communication and radar performances, the optimal function is to maximize the sum-rate of the system, with the constraints given by

$$\begin{aligned} \max \quad R_{\text{sum}} &= \sum_{k=1}^K \log_2(1 + \gamma_k) + \log_2(1 + \gamma_T) \\ &= \log_2 \text{Det}(\mathbf{I}_{K+1} + \mathbf{\Gamma}_{K+1}). \end{aligned} \quad (17)$$

s.t. $C1 : \gamma_k \geq 2^{\rho_k} - 1, \forall k,$
 $C2 : \gamma_T \geq 2^{\rho_T} - 1,$
 $C3 : P_T + \sum_{k=1}^K P_k \leq P_{\text{tot}},$

where P_{tot} is the total transmit power of the BS, ρ_k and ρ_T are respectively the thresholds of the required SINR of UE and TA. $\mathbf{\Gamma}_{K+1} = \text{Diag}[\gamma_1, \gamma_2, \dots, \gamma_K, \gamma_T]$ is a diagonal matrix.

There are three constraints. $C1$ is to certify the communication the quality of service (QoS) requirement of each UE. $C2$ is used to ensure the TA detection, and the radar rate R_{rad} should be larger than the threshold ρ_T . $C3$ is the total power constraint.

Obviously, the optimization issue is non-convex. Therefore, we propose a sub-optimal joint resource allocation algorithm, including two parts: user selection, and precoding & processing design with power allocation. It is noted that the UE’s weight \mathbf{w}_k is constant, while the TA’s weight \mathbf{w}_T is various during different M blocks. The user selection part is to select K UEs from the user set, so that to maximize R_{com} . Based on the selected UEs, the power allocation algorithm is designed to acquire \mathbf{W} and \mathbf{V} to obtain the sub-optimal solution of (17).

C. Sub-issue: user selection

This part is discussed based on a given \mathbf{W} . We adopt MRT precoding as the initial iteration value, where $\mathbf{W}_{\text{MRT}} = \mathbf{H}^H$ and the subscript ‘‘MRT’’ indicates maximum ratio transmission (MRT) [38]. Note that the user selection result will not affect the design of \mathbf{W} . Actually, γ_k is mainly determined by each UE’s θ_k and φ_k . Define $\Psi = \{q_1, q_2, \dots, q_u, \dots, q_U\}$ and $\psi = \{q_{i_1}, q_{i_2}, \dots, q_{i_k}, \dots, q_{i_K}\}$ by the sets of all the UEs and the selected served UEs respectively, where $1 \leq i_1 < i_2 < \dots < i_K \leq U$. Obviously, ψ is a subset of Ψ , i.e., $\psi \subseteq \Psi$. The optimal user selection algorithm is traversal algorithm, and its complexity is defined by the size of user set, which is $\mathcal{O}(U^K)$ complex multiplications. If U and K are small, the traversal algorithm is appreciated. However, when U and K are large,

Algorithm 1 Successive maximum iteration user selection algorithm

Input: $\Psi, G_u, d_u, \alpha, \delta_u, \mathbf{a}_t(\theta_u, \varphi_u)$
Output: ψ

```

1: Initialization  $K$  and  $M$ .
2: for  $m = 1 : M$ 
3:    $\mathbf{w}_T = \text{vec}(\mathbf{a}_{tx}^T(\theta_m, \varphi_m)\mathbf{a}_{ty}(\theta_m, \varphi_m)) \in \mathbb{C}^{1 \times N_t}$ 
4:   when  $K < U$ 
5:     Calculate  $\mathbf{h}_u = \sqrt{(d_u/d_0)^{-\alpha} \delta_u} \mathbf{a}_t(\theta_u, \varphi_u)$ .
6:     Let  $\mathbf{w}_u = \mathbf{h}_u^H$ .
7:     for  $k = 1 : K$ 
8:       for  $q_u \in \Psi$ 
9:         Let  $\psi = \psi + \{q_u\}$ .
10:        Calculate  $c_k = \max_{\psi} \sum \log_2(1 + \gamma_u)$ .
11:      end
12:      if  $c_k > c_{\Delta}$ 
13:        Select the UE  $q_{i_k} = \arg c_k$ .
14:        Update  $c_{\Delta} = c_k, \Psi = \Psi - \{q_{i_k}\}$  and  $\psi =$ 
         $\psi + \{q_{i_k}\}$ .
15:      else
16:        Output the selected UE set  $\psi$ .
17:      end
18:    end
19: end
    
```

the complexity will increase dramatically. Thus, it is important to present an algorithm to reduce the algorithm complexity.

This paper proposes a low complexity sub-optimal user selection algorithm, named as successive maximum iteration (SMI) user selection algorithm. The main idea behind SMI is to select the UE who can provide the maximum R_{com} during each iteration. Then, the selected UE is removed from the user set, and goes to the next selection step. The iteration is repeated, until all the K UEs are selected. Thus, the complexity of SMI is $\mathcal{O}(UK)$, which is much lower than that of the traversal method. The SMI is shown in Algorithm 1.

D. Sub-issue: precoder and processor design with power allocation

In the following discussion, assume the UEs have been selected, and the CSI of the selected K UEs are known. Moreover, suppose there exists a TA at the location of the m th block time. It is well known that the Lagrange multiplier method (LM) [39] is one of the most popular algorithm to solve the optimization issue. However, the proposed issue is non-convex, thus, we explore the majorization minimization algorithm (MM) [40] with the Lagrange multiplier method, i.e. maximum minimization Lagrange multiplier algorithm (MMLM), to solve our problem.

The MM procedure consists of two stages. The first stage is to find a surrogate function, which is simple and solvable. Then, we minimize the gap between the original function and surrogate function at a specific point. Besides, the surrogate function is an upper bound of the objective function. The second stage is to minimize the surrogate function, and find

the optimal value, bringing the derived solutions for the next MM iteration. The procedure is repeated until reaching the maximum iteration number.

The key issue of applying MM is to find a surrogate function. In [39], it shows that the function $\log[\text{Det}(\mathbf{\Sigma})]$ can be given as

$$\log[\text{Det}(\mathbf{\Sigma})] \leq \log[\text{Det}(\mathbf{\Sigma}_0)] + \text{tr}(\mathbf{\Sigma}_0^{-1}(\mathbf{\Sigma} - \mathbf{\Sigma}_0)), \quad (18)$$

where $\mathbf{\Sigma}_0$ is a constant matrix, and the inequality strictly holds with $\mathbf{\Sigma} = \mathbf{\Sigma}_0$. The problem of (17) can reformulate as

$$\begin{aligned} \min \quad & -R_{\text{sum}} = \log_2 \left[\text{Det}(\mathbf{I}_{K+1} + \mathbf{\Gamma}_{K+1})^{-1} \right] \\ \text{s.t.} \quad & C1, C2, C3. \end{aligned} \quad (19)$$

Thus, (19) becomes

$$\begin{aligned} \log_2 \left[\text{Det}(\mathbf{I}_{K+1} + \mathbf{\Gamma}_{K+1})^{-1} \right] \leq \log_2 \left[\text{Det}(\mathbf{I}_{K+1} + \mathbf{\Gamma}_{MRT})^{-1} \right] \\ + \text{tr} \left[(\mathbf{I}_{K+1} + \mathbf{\Gamma}_{MRT})(\mathbf{\Gamma}_{K+1} - \mathbf{\Gamma}_{MRT})^{-1} \right], \end{aligned} \quad (20)$$

where $\mathbf{\Gamma}_{MRT}$ is the diagonal matrix as aforementioned.

Our goal is to minimize the right side of (20). Since $\mathbf{\Gamma}_{MRT}$ is a constant matrix, the problem is equivalent to maximize the trace of $\mathbf{\Gamma}_{K+1}$, as

$$\begin{aligned} \max \quad & \text{tr}(\mathbf{\Gamma}_{K+1}) = \sum_{k=1}^K \gamma_k + \gamma_T \\ \text{s.t.} \quad & C1, C2, C3. \end{aligned} \quad (21)$$

Obviously, (21) is a convex function, which can be solved by Lagrange multiplier method. Define Lagrange function as

$$\begin{aligned} L(\mathbf{W}, \mathbf{V}, \boldsymbol{\eta}) = \sum_{k=1}^K \left[(1 + \eta_k) \gamma_k + \eta_k (1 - 2^{\rho_k}) \right] \\ + (1 + \eta_T) \gamma_T + \eta_T (1 - 2^{\rho_T}) + \eta_P \left(\sum_{k=1}^K P_k + P_T - P_{\text{tot}} \right), \end{aligned} \quad (22)$$

where $\boldsymbol{\eta} = [\eta_1, \dots, \eta_K, \eta_T, \eta_P] \in \mathbb{C}^{1 \times (K+2)}$ is a vector of non-positive Lagrange multipliers. The Karush-Kuhn-Tucker (KKT) conditions [41] of (22) are

$$\frac{\partial L(\mathbf{W}, \mathbf{V}, \boldsymbol{\eta})}{\partial \mathbf{W}} = \mathbf{0}, \quad (22a)$$

$$\frac{\partial L(\mathbf{W}, \mathbf{V}, \boldsymbol{\eta})}{\partial \mathbf{V}} = \mathbf{0}, \quad (22b)$$

$$\eta_v \leq 0, v \in \{1, 2, \dots, K, T, P\}, \quad (22c)$$

$$\gamma_v + 1 - 2^{\rho_v} \geq 0, \quad (22d)$$

$$\eta_v (\gamma_v + 1 - 2^{\rho_v}) = 0, \quad (22e)$$

$$\eta_P \leq 0, \quad (22f)$$

$$\sum_{k=1}^K P_k + P_T - P_{\text{tot}} \leq 0, \quad (22g)$$

$$\eta_P \left(\sum_{k=1}^K P_k + P_T - P_{\text{tot}} \right) = 0, \quad (22h)$$

where (22a) and (22b) can be extended as

$$\begin{aligned} \frac{\partial L(\mathbf{W}, \mathbf{V}, \boldsymbol{\eta})}{\partial \mathbf{w}_k} &= \frac{2(1 + \eta_k)P_k |\mathbf{h}_k \mathbf{w}_k| \mathbf{h}_k}{\left| \sqrt{P_T} \mathbf{h}_k \mathbf{w}_T + \sum_{i=1, i \neq k}^K \sqrt{P_i} \mathbf{h}_i \mathbf{w}_i \right|^2 + \sigma_k^2} \\ &- \sum_{\substack{i=1 \\ i \neq k}}^K \frac{2(1 + \eta_i)P_i |\mathbf{h}_i \mathbf{w}_i|^2 |\mathbf{h}_i \mathbf{w}_k| \mathbf{h}_i}{\left(\left| \sqrt{P_T} \mathbf{h}_i \mathbf{w}_T + \sum_{j=1, j \neq i}^K \sqrt{P_j} \mathbf{h}_j \mathbf{w}_j \right|^2 + \sigma_i^2 \right)^2} \\ &+ (1 + \eta_T) \cdot \frac{\mathcal{E}_{\text{rad}} \mathbf{V} \mathbf{Z} \frac{\partial(\mathbf{W} \mathbf{W}^H)}{\partial \mathbf{w}_k} \mathbf{Z}^H \mathbf{V}^H}{\mathbf{V} \mathbf{A}_K \mathbf{A}_K^H \mathbf{V}^H + \mathbf{V} \mathbf{V}^H \sigma^2}, \quad (23) \end{aligned}$$

$$\begin{aligned} \frac{\partial L(\mathbf{W}, \mathbf{V}, \boldsymbol{\eta})}{\partial \mathbf{V}} &= \left[\frac{(2\mathbf{Z} \mathbf{W} \mathbf{W}^H \mathbf{Z}^H \mathbf{V}^H)(\mathbf{V} \mathbf{A}_K \mathbf{A}_K^H \mathbf{V}^H + \mathbf{V} \mathbf{V}^H \sigma^2)}{(\mathbf{V} \mathbf{A}_K \mathbf{A}_K^H \mathbf{V}^H + \mathbf{V} \mathbf{V}^H \sigma^2)^2} \right. \\ &- \left. \frac{(\mathbf{V} \mathbf{Z} \mathbf{W} \mathbf{W}^H \mathbf{Z}^H \mathbf{V}^H)(2\mathbf{A}_K \mathbf{A}_K^H \mathbf{V}^H + 2\mathbf{V}^H \sigma^2)}{(\mathbf{V} \mathbf{A}_K \mathbf{A}_K^H \mathbf{V}^H + \mathbf{V} \mathbf{V}^H \sigma^2)^2} \right] \\ &\cdot (1 + \eta_T) \mathcal{E}_{\text{rad}}. \quad (24) \end{aligned}$$

To obtain the solutions of \mathbf{W} and \mathbf{V} in (22), we adopt the alternating direction method of multipliers (ADMM). The initialized \mathbf{W} by MRT is denoted by $\mathbf{W}^{(0)}$, where “0” indicates the initial step. Let $\frac{\partial L(\mathbf{W}^{(0)}, \mathbf{V}, \boldsymbol{\eta})}{\partial \mathbf{V}} = \mathbf{0}$, then it is derived that

$$\begin{aligned} \mathbf{Z} \mathbf{W}^{(0)} (\mathbf{W}^{(0)})^H \mathbf{Z}^H \mathbf{V}^H (\mathbf{V} \mathbf{A}_K \mathbf{A}_K^H \mathbf{V}^H + \mathbf{V} \mathbf{V}^H \sigma^2) &= \\ \mathbf{V} \mathbf{Z} \mathbf{W}^{(0)} (\mathbf{W}^{(0)})^H \mathbf{Z}^H \mathbf{V}^H (\mathbf{A}_K \mathbf{A}_K^H \mathbf{V}^H + \mathbf{V}^H \sigma^2). \quad (25) \end{aligned}$$

By solving (25), we can obtain $\mathbf{V}^{(1)}$ and then bring it to (22a).

Set $\frac{\partial L(\mathbf{W}, \mathbf{V}^{(1)}, \boldsymbol{\eta})}{\partial \mathbf{w}_k} = \mathbf{0}$, and achieve $\mathbf{W}^{(1)}$. According to the derived $\mathbf{V}^{(1)}$ and $\mathbf{W}^{(1)}$, do water filling power allocation algorithm to maximum the trace

$$\begin{aligned} \text{tr}(\mathbf{\Gamma}_{K+1}^{(1)}) &= \sum_{k=1}^K \frac{P_k |\mathbf{h}_k \mathbf{w}_k^{(1)}|^2}{\left| \sqrt{P_T} \mathbf{h}_k \mathbf{w}_T^{(1)} + \sum_{i=1, i \neq k}^K \sqrt{P_i} \mathbf{h}_i \mathbf{w}_i^{(1)} \right|^2 + \sigma_k^2} \\ &+ \frac{\mathcal{E}_{\text{rad}} \mathbf{V}^{(1)} \mathbf{Z} \mathbf{W}^{(1)} (\mathbf{W}^{(1)})^H \mathbf{Z}^H \mathbf{V}^{(1)H}}{\mathbf{V}^{(1)} \mathbf{A}_K \mathbf{A}_K^H \mathbf{V}^{(1)H} + \mathbf{V}^{(1)} \mathbf{V}^{(1)H} \sigma^2}, \quad (26) \end{aligned}$$

and the optimal power allocation results $P_k^{(1)}$ and $P_T^{(1)}$ can be obtained.

Following, take $\mathbf{V}^{(1)}$ and $\mathbf{W}^{(1)}$ into (20), and obtain the next surrogate function. By optimizing the new surrogate function, we can solve $\mathbf{V}^{(2)}$ and $\mathbf{W}^{(2)}$ by KKT conditions, and then do water filling power allocation to maximize $\text{tr}(\mathbf{\Gamma}_{K+1}^{(2)})$. Repeat this process, until the iteration number i reaches the maximum iteration number ν_{max} , or satisfying $\|\mathbf{W}^{(i)} - \mathbf{W}^{(i-1)}\|^2 < \varepsilon$ and $\|\mathbf{V}^{(i)} - \mathbf{V}^{(i-1)}\|^2 < \varepsilon$, where ε is a small position number, i.e., 10^{-3} . Finally, we can obtain the solutions $\mathbf{W} = \mathbf{W}^{(\nu_{max})}$ and $\mathbf{V} = \mathbf{V}^{(\nu_{max})}$, and the power allocation results $P_k^{(\nu_{max})}$ and $P_T^{(\nu_{max})}$, where ν_{max} is the final iteration times. The MMLM is presented in Algorithm 2.

As a summary, the joint resource allocation algorithm includes user selection, and precoder and processor design with power allocation. During the initialization, we firstly do SMI to find the UE set ψ , then utilize MMLM to calculate \mathbf{W} , \mathbf{V} , P_T and P_k . Overall, the whole algorithm needs at least $(UK\nu_{max})$ complex multiplications.

Algorithm 2 Maximum minimization Lagrange multiplier algorithm for designing \mathbf{W} and \mathbf{V}

Input: ψ , γ_k , γ_T , ρ_k , ρ_T , ε , ν_{max}

Output: \mathbf{W} and \mathbf{V}

- 1: **Initialization** $\mathbf{W}^{(0)}$ by MRT precoding.
- 2: **Set** $i = 1$, ε and ν_{max} .
- 3: **while** $i < N_{ite}$ & $\|\mathbf{W}^{(i)} - \mathbf{W}^{(i-1)}\|^2 \geq \varepsilon$ & $\|\mathbf{V}^{(i)} - \mathbf{V}^{(i-1)}\|^2 \geq \varepsilon$
- 4: Find the surrogate function according to (20) and optimize the surrogate function.
- 5: Construct Lagrange function $L(\mathbf{W}^{(i)}, \mathbf{V}^{(i)}, \boldsymbol{\eta})$.
- 6: Calculate KKT conditions of (22).
- 7: Calculate $\mathbf{V}^{(i)}$ by $\frac{\partial L(\mathbf{W}^{(i-1)}, \mathbf{V}^{(i)}, \boldsymbol{\eta})}{\partial \mathbf{V}^{(i)}} = \mathbf{0}$ and bring it back to (23).
- 8: Calculate $\mathbf{w}_k^{(i)}$ by $\frac{\partial L(\mathbf{W}^{(i)}, \mathbf{V}^{(i)}, \boldsymbol{\eta})}{\partial \mathbf{w}_k^{(i)}} = \mathbf{0}$ and update KKT conditions.
- 9: Do water filling algorithm to maximize the trace $\text{tr}(\mathbf{\Gamma}_{K+1}^{(i)})$, acquire the optimal power allocation results $P_k^{(\nu_{max})}$ and $P_T^{(\nu_{max})}$.
- 10: **end**
- 11: $\mathbf{W} = \mathbf{W}^{(\nu_{max})}$ and $\mathbf{V} = \mathbf{V}^{(\nu_{max})}$

V. THEORETICAL ANALYSIS

In this section, we derive the spectrum, BER and AF of the proposed system.

A. Spectrum

Actually, the spectrum of the integrated signal is determined by the transmit signal $s_{n_t}(t)$. Since the spectrum of the band-pass and baseband signals are equivalent, we only consider the equivalent baseband signal $\hat{s}_{n_t}(t)$ of (3), which is given by

$$\begin{aligned} \hat{s}_{n_t}(t) &= \sum_{n=1}^N x_{n_t, n} g(t - (n-1)T_s) e^{j\pi \mu t^2}, \\ &= \sum_{n=1}^N \left(w_{n_t, T} e^{j \sum_{i=1}^n b_{T, i} h \pi} + \sum_{k=1}^K w_{n_t, k} e^{j \sum_{i=1}^n b_{k, i} h \pi} \right) \\ &\cdot g(t - (n-1)T_s) e^{j\pi \mu t^2}. \quad (27) \end{aligned}$$

Since the spectrum of different transmit antennas are the same, we take the n_t th antenna as an example for analyzing. Define the Fourier transform of $\hat{s}_{n_t}(t)$ by $\mathcal{S}(f)$, which can be expressed as

$$\begin{aligned} \mathcal{S}(f) &= \int_{-\infty}^{+\infty} \sum_{n=1}^N \left(w_{n_t, T} e^{j \sum_{i=1}^n b_{T, i} h \pi} + \sum_{k=1}^K w_{n_t, k} e^{j \sum_{i=1}^n b_{k, i} h \pi} \right) \\ &\cdot g(t - (n-1)T_s) e^{j\pi(\mu t^2 - 2ft)} dt, \\ &= \sum_{n=1}^N \left(w_{n_t, T} \cdot \prod_{i=1}^n e^{j b_{T, i} h \pi} + \sum_{k=1}^K w_{n_t, k} \cdot \prod_{i=1}^n e^{j b_{k, i} h \pi} \right) \\ &\cdot \int_0^{T_B} g(t) e^{j\pi(\mu t^2 - 2ft)} dt. \quad (28) \end{aligned}$$

$$|\mathcal{G}_{LFM}(f)| = \sqrt{\left[C \left(\sqrt{\mu} T_B - \frac{f}{\sqrt{\mu}} \right) + C \left(\frac{f}{\sqrt{\mu}} \right) \right]^2 + \left[S \left(\sqrt{\mu} T_B - \frac{f}{\sqrt{\mu}} \right) + S \left(\frac{f}{\sqrt{\mu}} \right) \right]^2}. \quad (33)$$

As mentioned in Section III, $b_{k,i}$ and $b_{T,i}$ are complex signals. Actually, the n th symbol of the n_t th transmit antenna $x_{n_t,n}$ is a random variable, thus the mean value of $x_{n_t,n}$ is

$$\begin{aligned} \mathbb{E}[|x_{n_t,n}|] &= \mathbb{E} \left[\left| w_{n_t,T} \prod_{i=1}^n e^{j b_{T,i} h \pi} + \sum_{k=1}^K w_{n_t,k} \prod_{i=1}^n e^{j b_{k,i} h \pi} \right| \right], \\ &= \left| w_{n_t,T} + \sum_{k=1}^K w_{n_t,k} \right| \frac{n}{\mathcal{M}} \sum_{\substack{\xi=-(\mathcal{M}-1) \\ \xi \text{ is odd}}}^{(\mathcal{M}-1)} e^{j \xi h \pi}, \end{aligned} \quad (29)$$

where ξ represents one of the \mathcal{M} values of the modulated independent symbols $b_{k,i}$ and $b_{T,i}$, and the prior probability of which is $\frac{1}{\mathcal{M}}$. From (29), it is found that different precoding schemes \mathbf{W} and modulation orders \mathcal{M} can affect the amplitude of the spectrum. Compared with MRT precoding, the spectrum of our scheme has a larger amplitude, and a smaller \mathcal{M} derives a lower amplitude. Assume

$$\begin{aligned} \mathcal{G}(f) &= \int_0^{T_B} g(t) e^{j\pi(\mu t^2 - 2ft)} dt, \\ &= \mathcal{G}_u(f) * \mathcal{G}_{LFM}(f), \end{aligned} \quad (30)$$

where $\mathcal{G}_u(f)$ is the Fourier transform of transmit pulse $g(t)$, and B_g is the bandwidth of $g(t)$. If we adopt rectangular pulse, i.e., $B_g = 1/T_s$ or raised-cosine pulse i.e., $B_g = (1 + \alpha_g)/2T_s$, where α_g is the roll-off factor.

Define $\mathcal{G}_{LFM}(f)$ by the Fourier transform of LFM signal, given by

$$\begin{aligned} \mathcal{G}_{LFM}(f) &= \int_0^{T_B} e^{j\pi(\mu t^2 - 2ft)} dt, \\ &= e^{-\frac{j\pi f^2}{\mu}} \int_{-\frac{f}{\sqrt{\mu}}}^{\sqrt{\mu} T_B - \frac{f}{\sqrt{\mu}}} \left[\cos(\pi t'^2) + j \sin(\pi t'^2) \right] dt', \end{aligned} \quad (31)$$

where $t' = \sqrt{\mu}t - \frac{f}{\sqrt{\mu}}$, $C(x) = \int_0^x \cos(\pi\alpha^2) d\alpha$ and $S(x) = \int_0^x \sin(\pi\alpha^2) d\alpha$ are cosine and sine Fresnel integral respectively. Since both $C(x)$ and $S(x)$ are odd function, the amplitude of $\mathcal{G}_{LFM}(f)$ can be expressed in (33).

According to (30), it is found that the integrated signal bandwidth is equal to $B = B_w + B_g$, i.e. $B = \mu T_B + 1/T_s$ for rectangular pulse or $B = \mu T_B + (1 + \alpha_g)/2T_s$ for raised-cosine pulse. To improve the spectrum efficiency, we can adopt bandwidth-saving pulse.

B. BER

Actually, the BER of the proposed system is independent of LFM. The optimum detector of a CPM signal is realized by Viterbi algorithm [42]. Considering the proposed system, the BER of the k th UE becomes

$$P_{e,k} = 2 \int_0^{+\infty} Q \left(\sqrt{\log_2 \mathcal{M} \left(1 - \frac{\sin 2\pi h}{2\pi h} \right) \gamma_k} \right) p(\gamma_k) d\gamma_k, \quad (34)$$

where $Q(x) = \int_x^{+\infty} \frac{1}{\sqrt{2\pi}} e^{-\frac{t^2}{2}} dt$, $p(\gamma_k)$ is the probability density function (PDF) of γ_k . For mathematic convenience, we utilize $\mathbf{W}^{(0)}$ that is obtained by MRT instead of the iteration optimal $\mathbf{W}^{(\nu_{max})}$ to calculate $p(\gamma_k)$. The expression of γ_k in (13) is

$$\gamma_k \leq \frac{P_k (d_k/d_0)^{-\alpha} \delta_k N_t}{\left| \sqrt{P_T} \mathbf{h}_k \mathbf{w}_T + \sum_{i=1, i \neq k}^K \sqrt{P_i} \mathbf{h}_k \mathbf{w}_i \right|^2 + \sigma_k^2}, \quad (35)$$

where the path loss $d_k^{-\alpha}$ and shadowing effect δ_k obey power law and log-normal distributions, the PDF of δ_k is $p(\delta_k) = \frac{1}{\delta_k \sqrt{2\pi\sigma_{\delta_k}^2}} e^{-\frac{\ln(\delta_k)^2}{2\sigma_{\delta_k}^2}}$, where σ_{δ_k} is the variance of δ_k .

Let $I_k = \sqrt{P_T} \mathbf{h}_k \mathbf{w}_T + \sum_{i=1, i \neq k}^K \sqrt{P_i} \mathbf{h}_k \mathbf{w}_i$ be the interferences, and it is the sum of several independent and identically (i.i.d) distributed random variables. According to the central limit theorem, I_k can be approximately viewed as complex Gaussian distribution, i.e., $\mathcal{N}(\mu_I, \sigma_I)$, which is simulated by Monte Carlo. The mean value of I_k can be derived by $\mu_I = \sqrt{P_T} \tilde{\mu}_T + \sum_{k=1}^K \sqrt{P_i} \tilde{\mu}_k$, where $\tilde{\mu}_T$ and $\tilde{\mu}_k$ are respectively the mean value of $\mathbf{h}_k \mathbf{w}_T$ and $\mathbf{h}_k \mathbf{w}_i$. It can be seen that a larger K leads to a larger mean value μ_I when the power allocation factor is fixed. Moreover, for a given K , e.g., $K = 4$, P_T shows a significant influence on the μ_I , indicating that the interference increases with the increased of P_T . The variance of I_k can be expressed as $\sigma_I = P_T \tilde{\sigma}_T + \sum_{k=1}^K P_i \tilde{\sigma}_k$, where $\tilde{\sigma}_T$ and $\tilde{\sigma}_k$ are respectively the variance of interference $\mathbf{h}_k \mathbf{w}_T$ and $\mathbf{h}_k \mathbf{w}_i$. Thus, the total interference plus noise obeys chi-square distribution with degree of freedom 2, given by

$$p(I_k) = \frac{1}{2\sigma_I^2} e^{-\frac{I_k}{2\sigma_I^2}}. \quad (36)$$

Assume $z_k = \frac{d_k^{-\alpha} \delta_k}{I_k}$, according to the relationship of product and quotient of random variables, the PDF of γ_k is

$$p(\gamma_k) = \frac{(2(\sigma_I + \sigma_k)^2)^{-\frac{1}{\alpha}} e^{\frac{\sigma_k^4}{2\sigma_I^2}}}{\alpha(d_{k,2} - d_{k,1})} Q \left(-\frac{\sigma_k}{2} \right) \Gamma \left(1 - \frac{1}{\alpha} \right) \gamma_k^{-\frac{1}{\alpha}-1}, \quad (37)$$

where $\Gamma(x) = \int_0^{+\infty} t^{x-1} e^{-t} dt$, $d_{k,1}$ and $d_{k,2}$ are respectively the minimum and maximum range from the BS to the k th UE, i.e. $d_{k,1} \leq d_k \leq d_{k,2}$.

Taking (37) into (34), we can derive the upper bound of the BER expression. Unfortunately, the closed-form solution can not be deducted since the integral of the Q function can be expressed by the analytical form.

C. AF

The ambiguity function is defined as the time-frequency response observed at the matched filter of the BS receiver, which is given by [43]

$$|\chi(\tau, fd)|^2 = \left| \int_{-\infty}^{+\infty} \tilde{s}_{n_t}(t) \tilde{s}_{n_t}^*(t - \tau) e^{j2\pi f a t} dt \right|^2, \quad (38)$$

$$|\chi(\tau, f_d)|^2 = \left| e^{-j\pi\mu\tau^2} \sum_{n=1}^N \sum_{i=1}^N \int_{-\infty}^{+\infty} x_{n_t, n} x_{n_t, i}^* g(t - (n-1)T_s) g^*(t - (i-1)T_s - \tau) e^{j2\pi(\mu\tau + f_d)t} dt \right|^2. \quad (41)$$

where $\tilde{s}_{n_t}(t)$ is the complex envelope of baseband signal $\hat{s}_{n_t}(t)$, substituting (27) into (38) yields (41).

Let $t_1 = t - (n-1)T_s$, $q = n - i$, (41) becomes

$$|\chi(\tau, f_d)|^2 = \left| e^{-j\pi\mu\tau^2} \sum_{n=1}^N e^{j2\pi(\mu\tau + f_d)(n-1)T_s} \cdot \sum_{i=1}^N \chi_1(\tau - qT_s, f_d + \mu\tau) \right|^2, \quad (42)$$

where

$$\chi_1(\tau - qT_s, f_d + \mu\tau) = \int_{-\infty}^{+\infty} x_{n_t, n} x_{n_t, i}^* g(t_1) g^*(t_1 - (\tau - qT_s)) e^{j2\pi(\mu\tau + f_d)t_1} dt_1, \quad (43)$$

is the single pulse auto-correlation function.

Let $g(t)$ be a rectangular pulse, regarding as the symmetry property, i.e., $|\chi(\tau, f_d)|^2 = |\chi(-\tau, -f_d)|^2$, (43) becomes

$$|\chi(\tau, f_d)|^2 = \left| \sum_{q=-(N-1)}^{(N-1)} \frac{\sin[\pi(f_d + \mu\tau)(N - |q|)T_s]}{\sin[\pi(f_d + \mu\tau)T_s]} \cdot \chi_1(\tau - qT_s, f_d + \mu\tau) \right|^2, \quad (44)$$

Obviously, the AF is a two-dimensional function of τ and f_d , whose maximum value occurs at $(\tau, f_d) = (0, 0)$. The cut along in Doppler axis is by setting $\tau = 0$, indicating the resolution in the Doppler dimension, which is

$$|\chi(0, f_d)|^2 = \left| \sum_{q=-(N-1)}^{(N-1)} \frac{\sin[\pi f_d(N - |q|)T_s]}{\sin(\pi f_d T_s)} \chi_1(-qT_s, f_d) \right|^2. \quad (45)$$

Set $|\chi(0, f_d)|^2 = 0$, the first null in Doppler domain occurs at $f_{d,w} = \frac{1}{NT_s}$. Similarly, the cut along in latency axis is obtained by setting $f_d = 0$, indicating the resolution in the latency dimension, which is

$$|\chi(\tau, 0)|^2 = \left| \sum_{q=-(N-1)}^{(N-1)} \frac{\sin[\pi\mu\tau(N - |q|)T_s]}{\sin(\pi\mu\tau T_s)} \chi_1(\tau - qT_s, \mu\tau) \right|^2. \quad (46)$$

Let $|\chi(\tau, 0)|^2 = 0$, the first null in latency domain occurs at $\tau_w = \frac{1}{\mu NT_s} = \frac{1}{B_w}$. It can be seen that τ_w is completely determined by the LFM sweep bandwidth. Define κ by the compression ratio of the transmit and received pulse duration, which is

$$\kappa = \frac{T_B}{\tau_w} = T_B B_w. \quad (47)$$

κ is the multiplication of block time and sweep bandwidth, which is also called time-bandwidth product [44]. The minimum detection distance is denoted by $d_{\min} = \frac{c}{2B_w}$, indicating the range resolution, and c is the speed of light. Similarly,

TABLE I: Simulation parameters

Significance	Parameters	Values
Number of UEs	K	4
Number of transmit antennas	N_t	16
Number of received antennas	N_r	4
Number of blocks	M	324
Number of symbols per block	N	20
Symbol duration	T_s	5 μ s
Carrier Central frequency	f_c	2.4 GHz
Chirp rate	μ	10^{10}
Pass loss factor	α	3.0
Transmit power	P_{tot}	30 dBm
Reference range	d_0	100 m

the minimum detection velocity is defined by $v_{\min} = \frac{\lambda}{2T_B}$, reflecting the Doppler resolution.

According to d_{\min} and v_{\min} , the time-bandwidth product increases with the increased sweep bandwidth, which is different from the single carrier radar signal. Evidently, a large κ can meet both the requirements of the range resolution and Doppler resolution.

VI. SIMULATION RESULTS

In this section, we evaluate the performance of our proposed system through numerical simulations. The equipped transmit and received antennas of the BS are respectively 16 and 4, which are respectively structured by a 4×4 and 2×2 URA. All the UEs are uniform distribution in the cell, and the simulation parameters are listed in Table I.

A. Spectrum

Fig. 4 shows the spectrum of the proposed integrated signal, with various chirp rates and pulses. It can be seen that the bandwidth of integrated waveforms are determined by both sweep bandwidth B_w and transmit pulse bandwidth B_g , independent of the center frequency f_c . For a given μ , if B_w is small, the ripples are very evident. On contrast, the spectrum tends to be a rectangular profile with the increasing of B_w . Obviously, the bandwidth of a raised cosine pulse is smaller than that of a rectangular pulse, for a given T_s . Moreover, the chirp rate μ affects the bandwidth significantly, a larger μ may lead to a larger bandwidth, e.g., the bandwidth of the curve in $\mu = 5 \times 10^9$ is half of the $\mu = 1 \times 10^{10}$. Furthermore, for a given $g(t)$ and μ , the bandwidth of CPM is narrower than that of BPSK. From the spectrum, it is found that \mathbf{W} has no effect to the bandwidth of the proposed system, verifying the analysis.

B. BER

The average BER performance is shown in Fig. 5. When $K = 4$, $N_t = 16$ and $P_T = 0.1P_{tot}$, it can be seen that the proposed scheme achieves 10^{-3} when SNR is 20 dB. The theoretical curve is the upper bound, since γ_k can get the

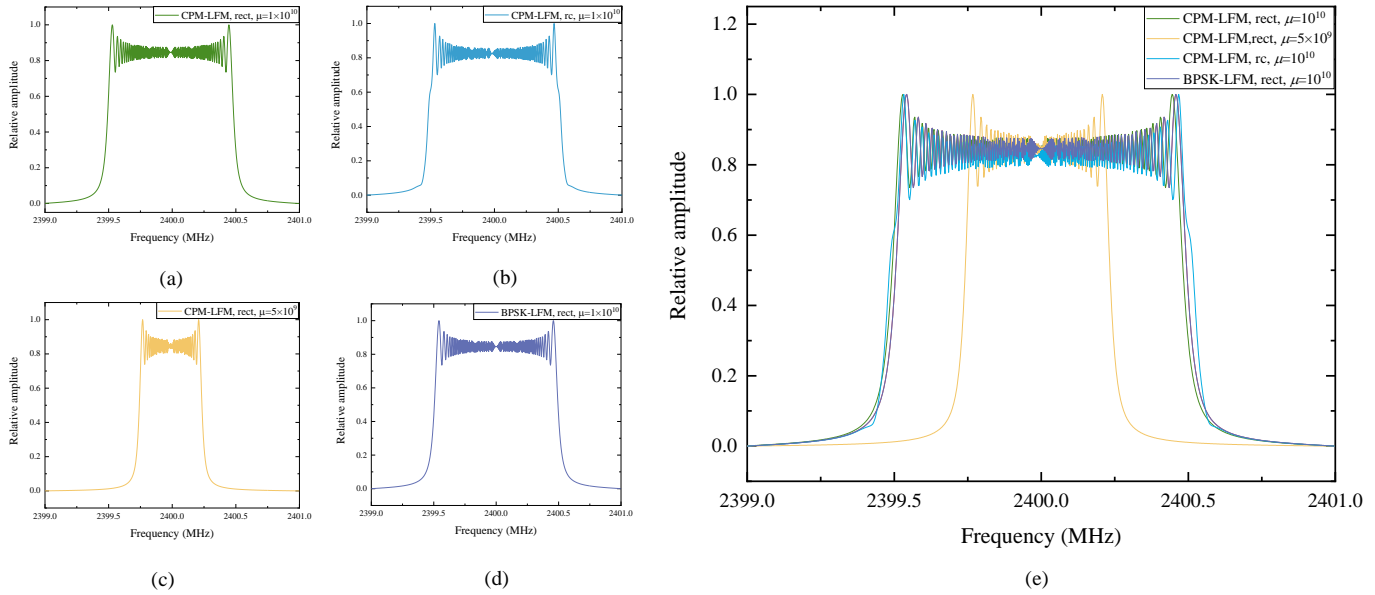


Fig. 4: Spectrum of the integrated signals with various chirp rates and pulses, where the subscript “rect” and “rc” represent the rectangular and raised-cosine pulse. (a) CPM-LFM signal with rectangular pulse, where $\mu = 1 \times 10^{10}$; (b) CPM-LFM signal with raised-cosine pulse, where $\mu = 1 \times 10^{10}$; (c) CPM-LFM signal with rectangular pulse, where $\mu = 5 \times 10^9$; (d) BPSK-LFM signal with rectangular pulse, where $\mu = 1 \times 10^{10}$; (e) overall spectrum comparison.

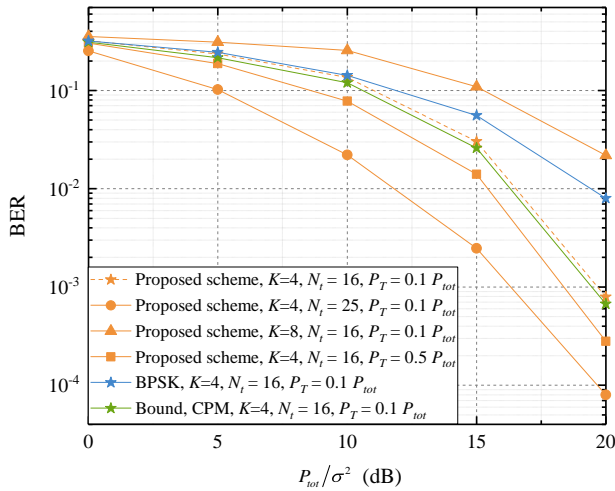


Fig. 5: The average BER versus P_{tot}/σ^2 in different modulation types, precoding schemes, number of UEs and number of transmit antennas.

maximum value. Moreover, when N_t is given, i.e., $N_t = 16$, a large K results in a worse BER performance because of the remaining interferences. In terms of the number of transmit antennas, a large N_t can eliminate the interferences effectively, providing a better BER performance. Furthermore, power allocation result also has an impact on the BER performance, since a larger P_T leads to the reduction of communication power P_k , indicating a deteriorated BER. As expected, when K , N_t and P_T are fixed, the proposed scheme provides better BER performance than BPSK counterpart, since the Viterbi algorithm is exploited for the CPM signal.

C. AF

The AF of our proposed system is shown in Fig 6, the horizontal and vertical axes stand for latency and Doppler frequency domains. When there is no TA exists, the peak of the AF is located at the $(\tau, f_d) = (0, 0)$. The location of the peak value is shifted with a moving TA, and located in the latency-Doppler domain. In (44), it can be seen that the AF is the combination of multiple spikes. The shape of each spike is determined by the transmit pulse type and precoding algorithm. Owing to the precoding methods, the peak of each spike becomes relative sharper than classical LFM signal, which exhibits a better range resolution. The corresponding zero-latency and zero-Doppler cuts are presented in (45) and (46). When $\tau = 0$ in (45) or $f_d = 0$ in (46), a larger symbol number N leads to a narrower $f_{d,w}$ or τ_w , indicating a smaller circle outline of each pulse, i.e., the better range and Doppler resolutions. Moreover, a larger μ leads to a larger sweep bandwidth B_w , which can increase the range resolution.

D. Sum-rate of the proposed DFRC system

The sum-rates of the proposed DFRC system are shown in Figs. 7-8. Fig. 7 shows the influence of \mathbf{W} , with the assumption $K = 4$; and Fig. 8 focuses on the impact of user selection algorithm.

According to the simulation parameters, the bandwidth of the radar system is five times larger than communication system, i.e. $B_w = 5 B_g$. To make a fair comparison, we should eliminate the influence of signal bandwidth and consider the sum-rate per bandwidth. It can be seen from Fig. 7, the proposed scheme has the best sum-rate performance than the pure communication or radar system. This is reasonable since there is a trade-off between the sum-rate per bandwidth

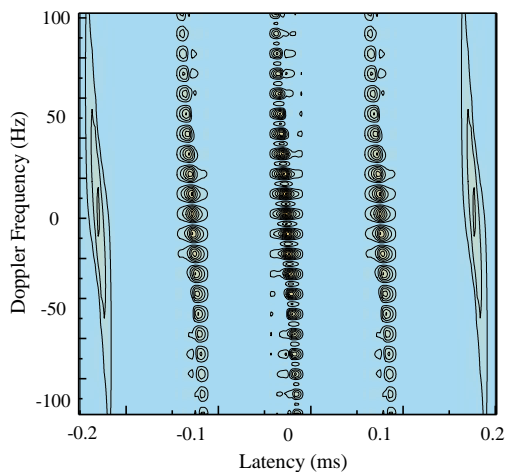


Fig. 6: The AF contour of our proposed system in latency and Doppler frequency domains, where $g(t)$ is rectangular pulse.

with the detection ability in radar system. Moreover, for the proposed JCR system, our designed \mathbf{W} provides the largest sum-rate than other classical beamforming algorithms, i.e., minimum mean square error (MMSE), followed by zero-forcing (ZF) and MRT. For example, when $\frac{P_{tot}}{\sigma^2} = 10$ dB, the sum-rate of our proposed scheme is 15.3 bps/Hz, which is approximately 2.1 bps/Hz, 2.5 bps/Hz and 2.8 bps/Hz larger than the MMSE, ZF and MRT algorithms.

From Fig. 8, it can be seen that the traversal user selection algorithm always provides the larger sum-rate than the proposed SMI algorithm, since it can achieve the optimal solution. Evidently, the complexity of SMI is much lower than the traversal algorithm, especially when U and K are large values. For example, when $U = 30$ and $K = 4$, the complexity of SMI is 120, while traversal algorithm is 8.1×10^5 . Moreover, M shows the impact on the TA detection precision. Let $\delta_\varphi = 10^\circ$, we compare the case $\delta_\theta = 10^\circ$ and $\delta_\theta = 15^\circ$, the corresponding $M = 324$ and 216. It can be derived that a larger M represents a higher sum-rate since it can enhance elevation or azimuth resolution, indicating the less interferences of each UE.

E. Trade-off between communication and radar performances

The relationship between the communication rate and detection range is shown in Fig. 9, where $K = 4, 6$ and RCS $\eta_T = 0.5, 0.8, 1.0 \text{ m}^2$. When K and η_T are constant, the communication rate decreases with the increased maximum detection range, since a larger detection range needs a larger P_{rad} , leading to a smaller P_{com} . It is remarkable that the influence of RCS can be ignored, when the detection distance is less than a threshold, i.e., 0.3. In the case $K = 4$ and $\eta_T = 0.5$, when the maximum detection range is 0.6 km, the communication rate is approximately 8.15 bps/Hz, while the maximum detection range is 0.8 km, the communication rate is 8.02 bps/Hz. The trade-off between the maximum detection range and the communication rate is mainly determined by the power allocation, since the total transmit power P_{tot} is a

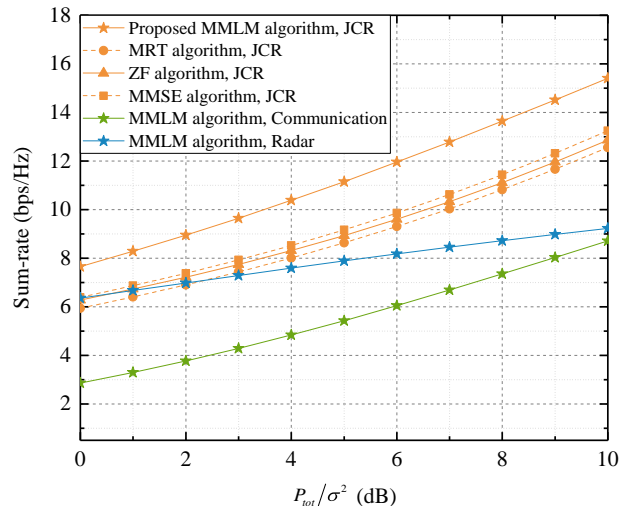


Fig. 7: An illustration of the sum-rate versus P_{tot}/σ^2 in proposed MMLM, ZF, MMSE, MRT algorithms in DFRC, pure communication and radar systems.

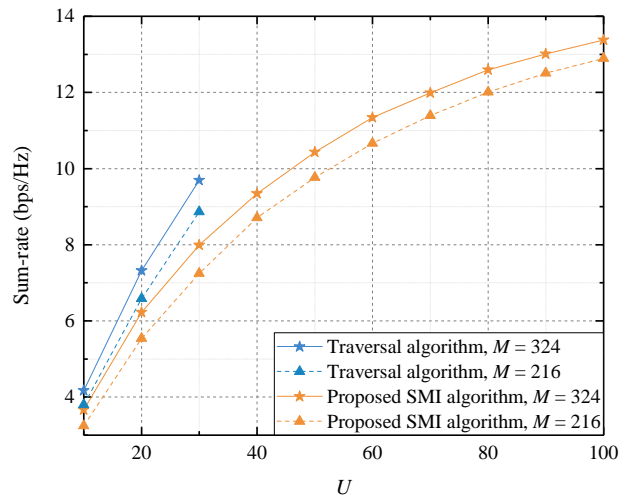


Fig. 8: An illustration of the sum-rate versus U in traversal and proposed SMI algorithm, where $M = 324$ and 216.

constant value, a better radar performance leads to a smaller communication rate.

VII. CONCLUSION

In this paper, we present a joint beamforming and CPM-LFM integrated signal, based on the proposed dual mode framework. The framework includes both dynamic mode and static mode, and the parameter M and N affect scanning precision and detection resolutions respectively. Following, we propose an objective function of sum-rate with constraints. To solve the non-convex issue, we give a sub-optimal joint beamforming and resource allocation algorithm, i.e. SMI-MMLM, which includes successive maximum iteration for user selection; and a maximum minimization Lagrange multiplier algorithm for precoding & processing design, with water filling algorithm to achieve the optimal power allocation results. Then, we give a detail analysis of the proposed

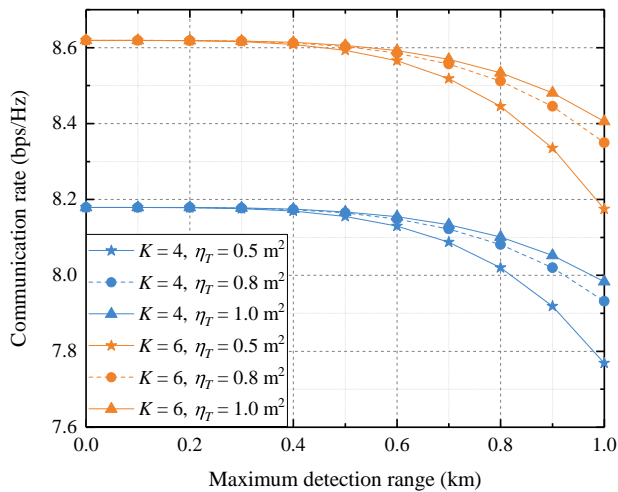


Fig. 9: Comparison between the communication rate versus maximum detection range in different user number K and RCS, where the chirp rate $\mu = 10^{10}$.

system, including the spectrum characteristic, BER and AF. Simulations results shows that our proposed CPM-LFM signal has better spectrum efficiency and range resolution. Moreover, the proposed SMI algorithm shows lower complexity than the optimal traversal algorithm, and the proposed MMLM algorithm performs larger sum-rate than the classical MRT, ZF and MMSE algorithms.

REFERENCES

- [1] W. L. van Rossum, J. J. M. de Wit, M. P. G. Otten and A. G. Huizing, "SMRF architecture concepts," *IEEE Aerosp. Electron. Syst. Mag.*, vol. 26, no. 5, pp. 12-17, May 2011.
- [2] F. Liu and C. Masouros, "A Tutorial on Joint Radar and Communication Transmission for Vehicular Networks—Part I: Background and Fundamentals," *IEEE Commun. Lett.*, vol. 25, no. 2, pp. 322-326, Feb. 2021.
- [3] X. Wang, Z. Fei, J. A. Zhang, J. Huang and J. Yuan, "Constrained Utility Maximization in Dual-Functional Radar-Communication Multi-UAV Networks," *IEEE Trans. Commun.*, vol. 69, no. 4, pp. 2660-2672, April 2021.
- [4] F. Liu and C. Masouros, "A Tutorial on Joint Radar and Communication Transmission for Vehicular Networks—Part II: State of the Art and Challenges Ahead," *IEEE Commun. Lett.*, vol. 25, no. 2, pp. 327-331, Feb. 2021.
- [5] P. Kumari, S. A. Vorobyov and R. W. Heath, "Adaptive Virtual Waveform Design for Millimeter-Wave Joint Communication-Radar," *IEEE Trans. Signal Process.*, vol. 68, pp. 715-730, 2020.
- [6] S. Quan, W. Qian, J. Guq and V. Zhang, "Radar-communication integration: An overview," in *Proc. The 7th IEEE/International Conference on Advanced Infocomm Technology*, Fuzhou, China, 2014, pp. 98-103.
- [7] R. Cager, D. LaFlame and L. Parode, "Orbiter Ku-Band Integrated Radar and Communications Subsystem," *IEEE Trans. Commun.*, vol. 26, no. 11, pp. 1604-1619, November 1978.
- [8] S. Sun, A. P. Petropulu and H. V. Poor, "MIMO Radar for Advanced Driver-Assistance Systems and Autonomous Driving: Advantages and Challenges," *IEEE Signal Process. Mag.*, vol. 37, no. 4, pp. 98-117, July 2020.
- [9] J. Wang, X. Liang, L. Chen, L. Wang and S. Shi, "Joint Wireless Communication and High Resolution SAR Imaging Using Airborne Mimo Radar System," in *Proc. IGARSS 2019 - 2019 IEEE International Geoscience and Remote Sensing Symposium*, Yokohama, Japan, 2019, pp. 2511-2514.
- [10] F. Liu, C. Masouros, A. P. Petropulu, H. Griffiths and L. Hanzo, "Joint Radar and Communication Design: Applications, State-of-the-Art, and the Road Ahead," *IEEE Trans. Commun.*, vol. 68, no. 6, pp. 3834-3862, June 2020.
- [11] S. Sodagari, A. Khawar, T. C. Clancy and R. McGwier, "A projection based approach for radar and telecommunication systems coexistence," in *Proc. 2012 IEEE Global Communications Conference (GLOBECOM)*, Anaheim, CA, USA, 2012, pp. 5010-5014.
- [12] J. Qian, M. Lops, Le Zheng, X. Wang and Z. He, "Joint System Design for Coexistence of MIMO Radar and MIMO Communication," *IEEE Trans. Signal Process.*, vol. 66, no. 13, pp. 3504-3519, July, 2018.
- [13] F. Liu, C. Masouros, T. Ratnarajah and A. Petropulu, "On Range Sidelobe Reduction for Dual-Functional Radar-Communication Waveforms," *IEEE Wireless Commun. Lett.*, vol. 9, no. 9, pp. 1572-1576, Sept. 2020.
- [14] F. Liu, L. Zhou, C. Masouros, A. Lit, W. Luo and A. Petropulu, "Dual-functional Cellular and Radar Transmission: Beyond Coexistence," in *Proc. 2018 IEEE 19th International Workshop on Signal Processing Advances in Wireless Communications (SPAWC)*, Kalamata, Greece, 2018, pp. 1-5.
- [15] B. Paul, A. R. Chiriyath and D. W. Bliss, "Survey of RF Communications and Sensing Convergence Research," *IEEE Access*, vol. 5, pp. 252-270, 2017.
- [16] A. Hassanien, M. G. Amin, Y. D. Zhang and F. Ahmad, "Dual-Function Radar-Communications: Information Embedding Using Sidelobe Control and Waveform Diversity," *IEEE Trans. Signal Process.*, vol. 64, no. 8, pp. 2168-2181, April 15, 2016.
- [17] F. Liu, L. Zhou, C. Masouros, A. Li, W. Luo and A. Petropulu, "Toward Dual-functional Radar-Communication Systems: Optimal Waveform Design," *IEEE Trans. Signal Process.*, vol. 66, no. 16, pp. 4264-4279, 15 Aug. 15, 2018.
- [18] F. Liu, C. Masouros, A. Li, H. Sun and L. Hanzo, "MU-MIMO Communications With MIMO Radar: From Co-Existence to Joint Transmission," *IEEE Trans. Wirel. Commun.*, vol. 17, no. 4, pp. 2755-2770, April 2018.
- [19] W. Yuan, F. Liu, C. Masouros, J. Yuan, D. W. K. Ng and N. González-Prelcic, "Bayesian Predictive Beamforming for Vehicular Networks: A Low-Overhead Joint Radar-Communication Approach," *IEEE Trans. Wirel. Commun.*, vol. 20, no. 3, pp. 1442-1456, March 2021.
- [20] Z. Cheng, B. Liao and Z. He, "Hybrid Transceiver Design for Dual-Functional Radar-Communication System," in *Proc. 2020 IEEE 11th Sensor Array and Multichannel Signal Processing Workshop (SAM)*, Hangzhou, China, 2020, pp. 1-5.
- [21] X. Liu, T. Huang, N. Shlezinger, Y. Liu, J. Zhou and Y. C. Eldar, "Joint Transmit Beamforming for Multiuser MIMO Communications and MIMO Radar," *IEEE Trans. Signal Process.*, vol. 68, pp. 3929-3944, 2020.
- [22] S. Quan, W. Qian, J. Guq and V. Zhang, "Radar-communication integration: An overview," in *Proc. The 7th IEEE/International Conference on Advanced Infocomm Technology*, Fuzhou, China, 2014, pp. 98-103.
- [23] H. Yang et al., "Queue-Aware Dynamic Resource Allocation for the Joint Communication-Radar System," *IEEE Trans. Veh. Technol.*, vol. 70, no. 1, pp. 754-767, Jan. 2021.
- [24] X. Chen, Z. Feng, Z. Wei, P. Zhang and X. Yuan, "Code-Division OFDM Joint Communication and Sensing System for 6G Machine-type Communication," *IEEE Internet of Things Journal*.
- [25] Y. Zhang, Q. Li, L. Huang, C. Pan and J. Song, "A Modified Waveform Design for Radar-Communication Integration Based on LFM-CPM," in *Proc. 2017 IEEE 85th Vehicular Technology Conference (VTC Spring)*, Sydney, NSW, Australia, 2017, pp. 1-5.
- [26] L. Huimin and Z. Jingya, "Analysis of a combined waveform of linear frequency modulation and phase coded modulation," in *Proc. 2016 11th International Symposium on Antennas, Propagation and EM Theory (ISAPE)*, Guilin, China, 2016, pp. 539-541.
- [27] Q. Li, K. Dai, Y. Zhang and H. Zhang, "Integrated Waveform for a Joint Radar-Communication System With High-Speed Transmission," *IEEE Wireless Commun. Lett.*, vol. 8, no. 4, pp. 1208-1211, Aug. 2019.
- [28] C. Sahin, J. Jakabosky, P. M. McCormick, J. G. Metcalf and S. D. Blunt, "A novel approach for embedding communication symbols into physical radar waveforms," in *Proc. 2017 IEEE Radar Conference (RadarConf)*, Seattle, WA, 2017, pp. 1498-1503.
- [29] S. Sharma, M. Melvasalo and V. Koivunen, "Multicarrier DS-CDMA Waveforms for Joint Radar-Communication System," in *Proc. 2020 IEEE Radar Conference (RadarConf20)*, Florence, Italy, 2020, pp. 1-6.
- [30] H. Chahrouh, S. Rajan, R. Dansereau and B. Balaji, "Hybrid beamforming for interference mitigation in MIMO radar," in *Proc. 2018 IEEE Radar Conference (RadarConf18)*, Oklahoma City, OK, USA, 2018, pp. 1005-1009.
- [31] X. Liu, T. Huang, N. Shlezinger, Y. Liu, J. Zhou and Y. C. Eldar, "Joint Transmit Beamforming for Multiuser MIMO Communications and MIMO Radar," *IEEE Trans. Signal Process.*, vol. 68, pp. 3929-3944, 2020.

- [32] P. Heidenreich, A. M. Zoubir and M. Rubsamen, "Joint 2-D DOA Estimation and Phase Calibration for Uniform Rectangular Arrays," *IEEE Trans. Signal Process.*, vol. 60, no. 9, pp. 4683-4693, Sept. 2012.
- [33] R. L. Maw and D. P. Taylor, "Space-Time Coded Systems using Continuous Phase Modulation," *IEEE Trans. Commun.*, vol. 55, no. 11, pp. 2047-2051, Nov. 2007.
- [34] N. J. Baas and D. P. Taylor, "Pulse shaping for wireless communication over time- or frequency-selective channels," *IEEE Trans. Commun.*, vol. 52, no. 9, pp. 1477-1479, Sept. 2004.
- [35] J. Zheng, H. Liu and Q. H. Liu, "Parameterized Centroid Frequency-Chirp Rate Distribution for LFM Signal Analysis and Mechanisms of Constant Delay Introduction," *IEEE Trans. Signal Process.*, vol. 65, no. 24, pp. 6435-6447, 15 Dec.15, 2017.
- [36] Y. Gu and A. Leshem, "Robust Adaptive Beamforming Based on Interference Covariance Matrix Reconstruction and Steering Vector Estimation," *IEEE Trans. Signal Process.*, vol. 60, no. 7, pp. 3881-3885, July 2012.
- [37] H. Li, Y.-W. Kiang, *The Electrical Engineering Handbook*, 2005.
- [38] S. Atapattu, P. Dharmawansa, C. Tellambura and J. Evans, "Exact Outage Analysis of Multiple-User Downlink With MIMO Matched-Filter Precoding," *IEEE Commun. Lett.*, vol. 21, no. 12, pp. 2754-2757, Dec. 2017.
- [39] Z. Cao, H. Guo, J. Zhang, D. Niyato and U. Fastenrath, "Improving the Efficiency of Stochastic Vehicle Routing: A Partial Lagrange Multiplier Method," *IEEE Trans. Veh. Technol.*, vol. 65, no. 6, pp. 3993-4005, June 2016.
- [40] Y. Sun, P. Babu and D. P. Palomar, "Majorization-Minimization Algorithms in Signal Processing, Communications, and Machine Learning," *IEEE Trans. Signal Process.*, vol. 65, no. 3, pp. 794-816, 1 Feb.1, 2017.
- [41] J. Liang, C. S. Leung and H. C. So, "Lagrange Programming Neural Network Approach for Target Localization in Distributed MIMO Radar," *IEEE Trans. Signal Process.*, vol. 64, no. 6, pp. 1574-1585, March15, 2016.
- [42] J. P. Fonseka, "Soft-decision phase detection with Viterbi decoding for CPM signals," *IEEE Trans. Commun.*, vol. 47, no. 12, pp. 1802-1810, Dec. 1999.
- [43] L. Zhang, B. Yang and M. Luo, "Joint Delay and Doppler Shift Estimation for Multiple Targets Using Exponential Ambiguity Function," *IEEE Trans. Signal Process.*, vol. 65, no. 8, pp. 2151-2163, 15 April15, 2017.
- [44] G. Chandran and J. S. Jaffe, "Signal set design with constrained amplitude spectrum and specified time-bandwidth product," *IEEE Trans. Commun.*, vol. 44, no. 6, pp. 725-732, June 1996.